

List-Mode Maximum Likelihood Reconstruction of Compton Scatter Camera Images in Nuclear Medicine¹

Scott J. Wilderman, N.H. Clinthorne, J.A. Fessler, and W. Les Rogers
University of Michigan

Abstract

A Maximum Likelihood (ML) image reconstruction technique using list-mode data has been applied to Compton scattering camera imaging. List-mode methods are appealing in Compton camera image reconstruction because the total number of data elements in the list (the number of detected photons) is significantly smaller than the number of possible combinations of position and energy measurements, leading to a much smaller problem than that faced by traditional iterative reconstruction techniques. For a realistic size device, the number of possible detector bins can be as large as 10 billion per pixel of the image space, while the number of counted photons would typically be a very small fraction of that. The primary difficulty in applying the list-mode technique is in determining the parameters which describe the response of the imaging system. In this work, a simple method for determining the required system matrix coefficients is employed, in which a back-projection is performed in list-mode, and response coefficients determined for only tallied pixels. Projection data has been generated for a representative Compton camera system by Monte Carlo simulation for disk sources with hot and cold spots and energies of 141, 364, and 511 keV, and reconstructions performed.

I. INTRODUCTION

Reconstruction of images from Compton aperture projection data is a computationally challenging task. To date, no exact, analytical solutions applicable to a practical imaging device have been found. Nor have traditional iterative reconstruction techniques (such as Maximum Likelihood (ML) Expectation Maximization (EM)), proven tractable, primarily because of the enormous size of the matrix required to describe a viable imaging system. For the C-SPRINT system [1] consisting of a 81 cm square scatter detector (with 1.2 mm spatial resolution and with energy recorded in 100 eV bins), and a cylindrical capture detector 25 cm in radius and 10 cm long (spatial resolution of 3 mm), the number of elements of the system matrix M_S is roughly 2.3×10^{10} per voxel of the image. For an $N \times N$ image, direct reconstruction in 2D would involve inversion of $M_S N^2$ dimensional matrices, and iterative methods would require $\sim 10^{14}$ recursive multiplications.

Since, in the general case, the number of detected events N_γ will be much smaller than the number of system elements M_S in the full projection data set, list-mode reconstruction methods present themselves as possible alternatives to other solution algorithms [2],[3]. In such methods, each event is

¹This work has been partially supported through Contract NCI 2RA01 CA-32846-24.

treated as a point in a continuous measurement space, rather than as contributing a count to a position and energy bin. Since $N_\gamma \ll M_S$, the sizes of the matrices are greatly reduced and so the number of operations required in solving the problem will be reduced by a like amount. In addition, this technique has the advantage of preserving accuracy of measurement data that might otherwise be lost in discretizing of energy and position during the binning procedure.

The conventional ML problem for the Compton camera can be posed as follows: Let Y be the measured projection data, accumulated in bins as the number of counts for a given combination of scatter detector element, capture detector element, and scattering energy bin (each bin is then denoted as Y_i), and $\underline{\lambda}$ the underlying pixelated object, each pixel having an intensity given by λ_j . Then (ignoring random coincidences)

$$Y \sim \text{Poisson}\{T\underline{\lambda}\}, \quad (1)$$

and the log-likelihood has the form

$$\log f(Y|\underline{\lambda}) = \sum_i Y_i \log \sum_j t_{ij} \lambda_j - \sum_i \sum_j t_{ij} \lambda_j. \quad (2)$$

In solving for $\underline{\lambda}$ using the iterative EM algorithm, the the maximization step can be written as

$$\frac{1}{\lambda_j} \sum_i Y_{ij}^E - s_j = 0 \quad (3)$$

and the expectation step as

$$Y_{ij}^E = Y_i \frac{\lambda_j t_{ij}}{\sum_k t_{ik} \lambda_k} \quad (4)$$

leading to the iteration

$$\lambda_j^{(l+1)} = \frac{\lambda_j^{(l)}}{s_j} \sum_i \frac{Y_i t_{ij}}{\sum_k t_{ik} \lambda_k^{(l)}}. \quad (5)$$

In the above, s_j is the probability that a photon emitted from pixel j would be detected anywhere, and the t_{ij} the probability that a γ emitted from pixel j is collected in bin i , so

$$s_j = \sum_i t_{ij}$$

Barrett *et al.* and Parra and Barrett [3, 4] have proven that the above expressions hold in the list-mode case, in which each detected event can be considered to be a unique bin (or the bins can be considered to be infinitesimally small - in either case $Y_i \rightarrow 1$) and the sums over the M_S system bins become sums

over just the N_γ detected events. The one exception is that as the Y_i no longer span the space of all possible detected events, $s_j \neq \sum_i t_{ij}$, but rather is now the integral over all possible events i , including those not measured in Y . It is noted that the t_{ij} above are equivalent to $p(\mathbf{A}_i|j)s_j$ in Parra's derivation, where \mathbf{A}_i are the measurements describing event Y_i .

As in all iterative methods, the primary difficulty method lies in generating the t_{ij} (and for the list-mode case, the s_j as well). In this paper we present a simple approximation for these probabilities and present images reconstructed from Monte Carlo simulations for a disks sources at a variety of energies.

II. METHODS

In a Compton scatter camera, the sequence of physical events which leads to a count being registered begins with the emission of a photon at \mathbf{z}_0 in direction Ω_0 , followed by Compton scattering at position \mathbf{z}_1 through an angle Ω_c (with energy loss E_c) and final absorption at \mathbf{z}_2 . The t_{ij} 's, the absolute probability that a photon emitted from j will give rise to event i described by the measured quantities \mathbf{z}_1, E_c , and \mathbf{z}_2 (henceforth denoted \mathbf{A}_i , after Parra), will be given by the integral over the area of pixel j of the product of the probabilities described below: (assuming a mono-energetic source):

$p(\mathbf{z}_0)d\mathbf{z}_0$, that the photon was emitted in $d\mathbf{z}_0$ at \mathbf{z}_0

$P(\Omega_0|\mathbf{z}_0)$, that it had initial direction Ω_0 in $d\Omega_0$ toward \mathbf{z}_1

$P_{escp}^{obj}(\mathbf{z}_0, \Omega_0)$, that it escaped the object

$p(\mathbf{z}_1|\mathbf{z}_0, \Omega_0)d\mathbf{z}_1$, that it Compton scattered in $d\mathbf{z}_1$ at \mathbf{z}_1

$P(\Omega_c|\mathbf{z}_1)$, that it emerged from the collision in direction $d\Omega_c$ at Ω_c subtended by \mathbf{z}_2

$p(E_c|\Omega_c)dE_c$, that it lost energy E_c in dE_c in the scattering collision

$P_{escp}^{det1}(\Omega_c, \mathbf{z}_1, E_c(\Omega_c))$, that it escaped the detector

$p_{abs}^{det2}(\mathbf{z}_2|\Omega_c, \mathbf{z}_1, E_c)d\mathbf{z}_2$, that it was absorbed in the second detector in $d\mathbf{z}_2$ at \mathbf{z}_2

The s_j 's are then integrals of the t_{ij} taken over both the scatter and capture detector areas and over the possible energies for the possible scattering angles.

Straightforward computation of either s_j or t_{ij} , which must take into account the finite position and energy resolution of the system, as well as Doppler broadening of the scattered photon energy distribution, is daunting. We instead begin by restricting ourselves to the $2D$ case, and argue that the s_j 's can be taken to be constant and have little impact on the estimates of λ . This assumption is reasonable because switching to $2D$ eliminates the major effect of attenuation in the object, and so variations in s_j will be limited primarily to solid angle issues. For small objects at moderate distances from the detectors, the s_j should vary slowly, and since errors in estimates of λ depend on the

roughness of the variations, the impact of this approximation should be fairly small. We next note that we can take

$$t_{ij} = p_{ij}^\dagger s_j \quad (6)$$

where the p_{ij}^\dagger are the probabilities (normalized to $\sum_j p_{ij}^\dagger = 1$) that a given event i emanated from an emission in pixel j . If we define $p(\mathbf{z}_0|\mathbf{A}_i)$ to be the probability of an emission having taken place in pixel element area $d_j(\mathbf{z}_0)$ for a given \mathbf{A}_i , we have

$$p_{ij}^\dagger = \int_j d_j(\mathbf{z}_0)p(\mathbf{z}_0|\mathbf{A}_i). \quad (7)$$

For the case of real measurements, we need to convolve the distribution $p(\mathbf{z}_0|\mathbf{A}_i')$ (we denote the exact parameters corresponding to the measurement $\mathbf{A}_i(\mathbf{z}_1, \mathbf{z}_2, \alpha_c)$ as $\mathbf{A}_i'(\mathbf{z}_1', \mathbf{z}_2', \alpha_c')$) with a function $p(\mathbf{A}_i|\mathbf{A}_i')$, where

$$H(\mathbf{A}_i|\mathbf{A}_i') = p(\mathbf{z}_1'|\mathbf{z}_1)p(\mathbf{z}_2'|\mathbf{z}_2)p(E_c'|E_c)p(E_c|\alpha_c).$$

The final factor here accounts for Doppler broadening, and the other conditional probabilities define the point spread function due to the errors in the measurement of the various components of \mathbf{A}_i' . We now claim that $p(\mathbf{z}_0|\mathbf{A}_i')$ can be determined by back-projecting the cone B_c determined by \mathbf{A}_i' , which traces out a conic section in the image plane. Only those points on the conic can be potential source points, \mathbf{z}_0 . This series of approximations is equivalent to Parra's application of Bayes' rule in deriving expressions for t_{ij} for $2D$ PET imaging [4], with the only difference being that $p(\mathbf{z}_0|\mathbf{A}_i')$ is described by the conic section rather than a δ function. Thus our general expression for t_{ij} is:

$$t_{ij} = s_j \int_j d_j(\mathbf{z}_0) \int d\mathbf{A}_i' p(\mathbf{z}_0|B_c(\mathbf{A}_i')) H(\mathbf{A}_i|\mathbf{A}_i'). \quad (8)$$

We can now either approximate $H(\mathbf{A}_i|\mathbf{A}_i')$ (which is not typically Gaussian for Compton imaging) so that the convolution can be determined analytically, or approximate the integral numerically. For the current work, we assume a perfect detector, $H(\mathbf{A}_i|\mathbf{A}_i') = \delta(\mathbf{A}_i - \mathbf{A}_i')$ and we perform a line integral over B_c , setting p_{ij}^\dagger to be s_j times the fraction of the total path of the located in pixel j :

$$p_{ij}^\dagger = \int_l d_j(\mathbf{z}_0) p_l(\mathbf{z}|B_c(\mathbf{A}_i)) / \sum_m \int_l d_m(\mathbf{z}_0) p_l(\mathbf{z}|B_c(\mathbf{A}_i)) \quad (9)$$

We obtain the the line integrals by performing the back-projection described in [5], approximating the the path of the back-projected cone i lying inside pixel j by straight line between the edge intercepts. The s_j are set arbitrarily, and the iteration in equation 5 can be performed.

III. RESULTS

Projection data was generated by Monte Carlo simulation using the program SKEPTIC [6]. SKEPTIC has been employed and tested extensively in numerous medical imaging

applications [7], [8], including simulation of Compton scatter cameras [1], [9]. The program writes to disk lists of the exact interaction positions and energy losses, and the uncertainties in the measurements of these quantities are simulated by sampling from appropriate Gaussian distributions describing the energy and spatial resolution of the component detectors, as described in [5]. Doppler broadening of the scattered gamma spectrum, which has recently been found to be a limiting factor in the resolution performance of Compton cameras [10], is modeled using the tabulated data of Biggs [11] for amorphous silicon and of Reed [12] for crystalline silicon. The list-mode reconstruction program reads this data and applies the back-projection algorithm of [9] to determine the coefficients t_{ij} , which are stored. The iterative procedure is then simple matrix multiplication. The detector system modeled is the C-SPRINT silicon and NaI system proposed by Clinthorne and LeBlanc [1]. It consists of a 9x9 cm array of Si elements, divided into 1.2 mm cells. Each cell is 5 mm thick and assumed to have an energy resolution of roughly 250 eV, (an achievable level, as suggested by Weilhammer [13]). The capture detector is taken to be a hollow cylinder of NaI, 25 cm in radius and 10 cm long, with a spatial resolution of 3 mm. ^{99m}Tc , and ^{131}I and annihilation photon sources were modeled. The test configuration was a 5 cm radius disk with uniform intensity 1, containing 2 hot spots (intensity 2) and 2 cold spots (intensity 0), of 1 and .5 cm radii, and a distance of 10 cm. Emission were sampled from continuous positions on the disk until 200,000 Compton events were collected. Reconstructions performed on a 32 by 32 grid of 5 mm pixels.

Results are shown below for all three test energies in figures 1 - 6. While the initial back-projection consumed roughly 10 minutes of CPU on a Ultra Sparc 1 workstation, subsequent iterations took just 30 seconds. At each energy, the first figure shows the image after the initial back-projection, and the second after 50-100 iterations. The quality of the images is degraded primarily by the limited number of counts and the impact of Doppler broadening on the approximations for t_{ij} . It should be noted that the geometry of the C-SPRINT detector tends to maximize the penalty due to the Doppler effect, which is most severe at the technetium energy. Nevertheless, in all 3 cases, both hot and both cold spots are in evidence.

Because of the relatively few number of counts, a smoothing penalty was introduced. Equation 3 is recast as

$$\frac{1}{\lambda_j} \sum_i Y_{ij}^E - s_j - \alpha \sum_k r_{jk} \lambda_k = 0. \quad (10)$$

Here the coefficients r_{jk} are 0 except for the 4 nearest and next nearest pixels k relative to j , and set so that $\sum_j \sum_k r_{jk} = 0$. The expectation step of equation 4 remains the same, but now the maximization step requires solving for a quadratic equation in λ_j (which roughly doubled the CPU usage per iteration). For the current work, α is set to some fraction α_0 times s_j/λ , the average value of λ . Some reconstructions are presented in figures 7 through 10 for α_0 ranging from 0.005 to 0.01. Image quality is greatly enhanced. are given in figures 7 through 9.

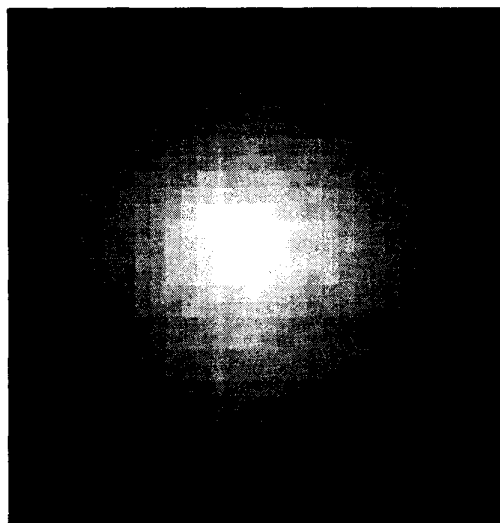


Figure 1: 141 keV Initial back-projected image

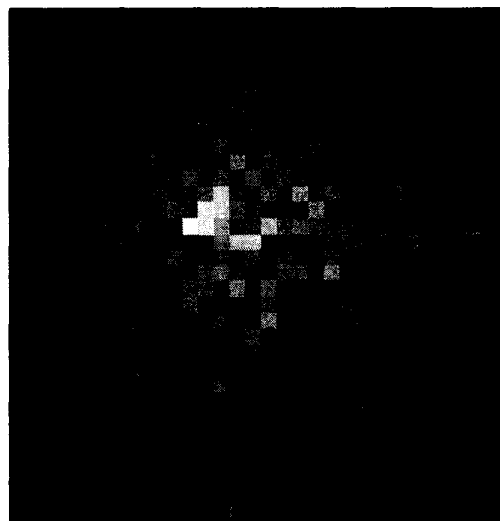


Figure 2: 141 keV Image after 75th iteration

IV. CONCLUSIONS

A list-mode maximum likelihood reconstruction algorithm has been applied to the Compton camera imaging problem in 2D with very good results over a wide range of energies, using a crude estimation of the system response matrix and a relative small number of counts. Improvements could be expected by approximating the conditional probabilities in 8, in the manner of [4], and by applying solid angle computations to weight the s_j 's. Future work should include parallelization of the algorithm to permit larger number of particles, and extension into 3D.

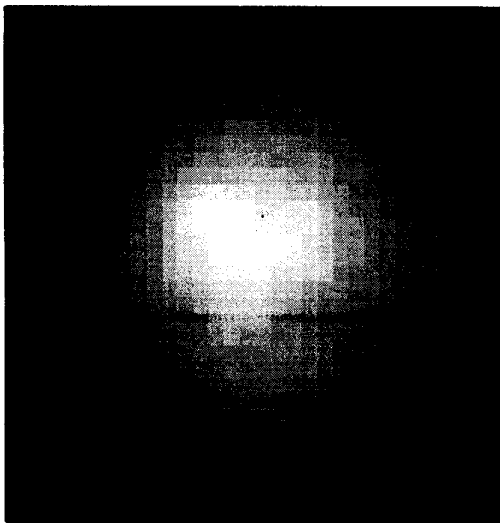


Figure 3: 364 keV Initial back-projected image

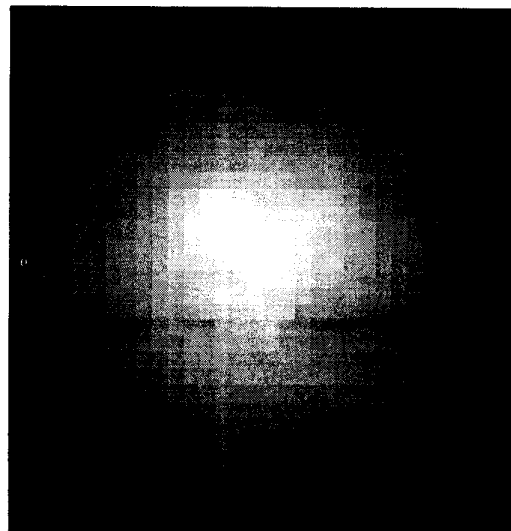


Figure 5: 511 keV Initial back-projected image



Figure 4: 364 keV Image after 75th iteration

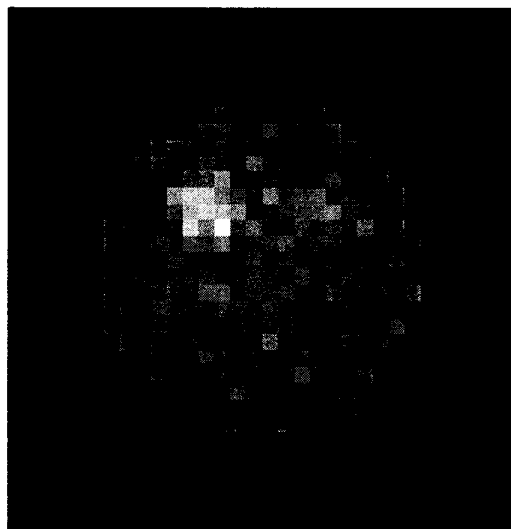


Figure 6: 511 keV Image after 65th iteration

V. REFERENCES

- [1] J.W. LeBlanc, N.H. Clinthorne, C-h. Hua, E. Nygard, W.L. Rogers, D.K. Wehe, P. Weilhammer, S.J. Wilderman, "C-Sprint: A prototype Compton camera system for low energy gamma ray imaging", presented at *IEEE Nucl. Sci. Sym. and Med. Imaging Conf., Albuquerque, N.M., 1997*.
- [2] T. Hebert, R. Leahy, M. Singh, "Three-dimensional maximum-likelihood reconstruction for an electronically collimated single-photon-emission imaging system," *J. Opt. Soc. Am.*, vol. 7, 1990 pp. 1305-1313.
- [3] H.H. Barrett, T. White, and L.C. Parra, "List-mode likelihood," *J. Opt. Soc. Am.*, vol. 14, 1997 pp. 2914-2923.
- [4] L.C. Parra and H.H. Barrett, "List-mode likelihood: EM

- algorithm and image quality estimation demonstrated on 2-D PET," *IEEE Trans. Med. Imag.*, vol. 17, 1998 pp. 228-235.
- [5] S.J. Wilderman, W.L. Rogers, G.F. Knoll and J.C. Engdahl, "Fast Algorithm for List-Mode Back-Projection of Compton Scatter Camera Data," *IEEE Trans. Nucl. Sci.*, in press.
- [6] S.J. Wilderman, "Vectorized algorithms for the Monte Carlo simulation of kilovolt electron and photon transport," *University of Michigan, Ann Arbor, MI, Ph. D. dissertation, 1990*.
- [7] M.J. Flynn, S.M. Hames, S.J. Wilderman, and J.J. Ciarelli, "Quantum noise in digital x-ray image detectors with

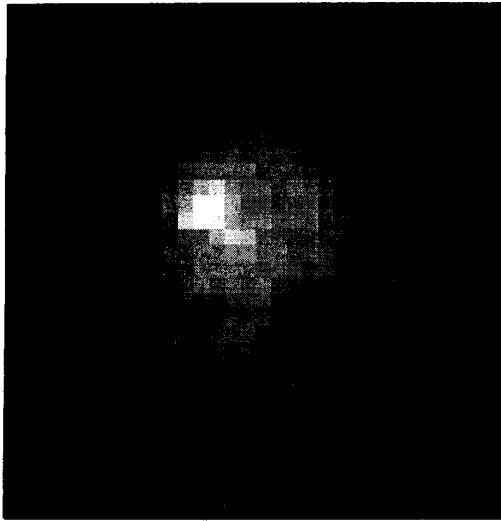


Figure 7: Smoothed ($\alpha_0 = 0.005$) 141 keV Image after 75th iteration

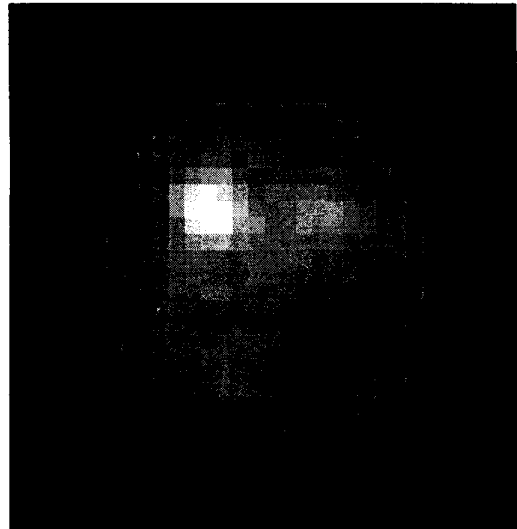


Figure 9: Smoothed ($\alpha_0 = 0.005$) 511 keV Image after 75th iteration

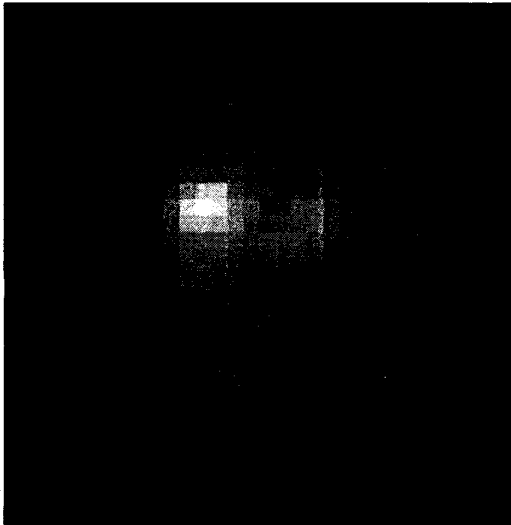


Figure 8: Smoothed ($\alpha_0 = 0.005$) 364 keV Image after 50th iteration

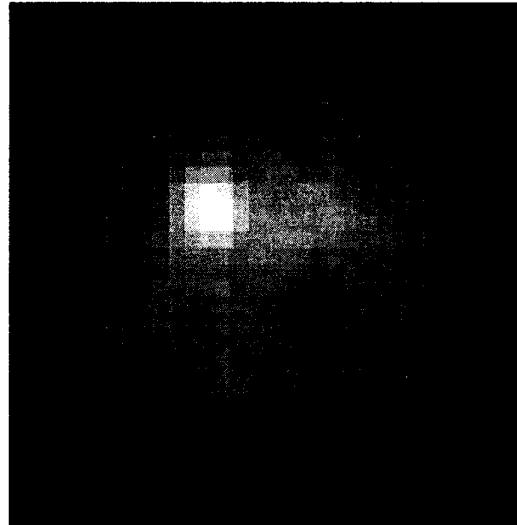


Figure 10: Smoothed ($\alpha_0 = 0.010$) 511 keV Image after 100th iteration

- optically coupled scintillators," *IEEE Trans. Nucl. Sci.*, vol. 43, 1996 pp. 2320-2325.
- [8] M.C. Wrobel, N.H. Clinthorne, J.A. Fessler, Y. Zhang, S.J. Wilderman, and W.L. Rogers, "Proposed method for correcting aperture penetration in high energy slit aperture and pinhole SPECT," *IEEE Trans. Nucl. Sci.*, vol. 44, 1997 pp. 1564-1570.
- [9] S.J. Wilderman, W.L. Rogers, G.F. Knoll and J.C. Engdahl, "Monte Carlo calculation of point spread functions of Compton scatter cameras," *IEEE Trans. Nucl. Sci.*, vol. 44, 1997 pp. 250-254.
- [10] C. Ordonez, A. Bolozdynya, and W. Chang, "Energy uncertainties in Compton scatter Cameras," presented at *IEEE Nucl. Sci. Sym. and Med. Imaging Conf.*, Albuquerque, N.M., 1997.
- [11] F. Biggs, L.B. Mendelsohn, and J.B. Mann, "Hartree-Fock Compton profiles for the elements," *At. Data Nuc. Data Tables*, vol. 16, 1975 pp. 201-309.
- [12] W.A. Reed and P. Eisenberger, "Gamma-ray Compton profiles of diamond, silicon, and germanium," *Phys. Rev. B*, vol. 6, 1972 pp. 4598-4604.
- [13] P. Weilhammer, *private communication*, Nov 1996.